



Engineering Notes

Optimal Aircraft Trajectories for Wind Energy Extraction

Yiming Zhao*

Halliburton Energy Services, Houston, Texas 77032

Atri Dutta†

Wichita State University, Wichita, Kansas 67260

and

Panagiotis Tsiotras‡ and Mark Costello§

Georgia Institute of Technology, Atlanta, Georgia 30332

DOI: 10.2514/1.G003048

I. Introduction

IT IS well known that birds and air vehicles are capable of extracting energy from atmospheric winds. Land birds such as condors and vultures remain aloft for hours at a time without flapping their wings. In straight and level flight, atmospheric wind updrafts rotate the relative aerodynamic velocity vector downward, causing the drag to point aft and slightly upward and the lift to point up and slightly forward. When the atmospheric wind updraft is sufficiently large, straight and level flight and even climbing flight are possible without power. Conventional sailplane soaring is based on this type of atmospheric wind energy extraction. Autonomous soaring has also been well researched, including flight-test experiments [1–5]. It is known for a long time that sea birds such as albatrosses and petrels are capable of extended flight over the sea without flapping their wings [6–10]. However, the physical mechanism in this case is fundamentally different from land birds. Seabirds extract energy from an atmospheric wind gradient near the surface of the ocean by alternating climbing and diving upwind and downwind of air masses moving at differing velocities. This type of atmospheric wind energy extraction is known as dynamic soaring and has been studied by a number of researchers, particularly for remote-control gliders flying near ridges [11–17].

In many practical scenarios, atmospheric wind energy in local regions is complex and does not fit neatly into a strict category of being an ideal thermal or wind shear. This paper investigates optimal energy-extracting trajectories in atmospheric wind shear for several scenarios, including altitude limited shear, direction changing shear, and negative shear. In the context of this paper, negative shear means that the wind speed drops as the altitude increases. To the best of the authors' knowledge, no bird is known to extract energy from negative wind shear in a sustainable manner, arguably because negative wind shear

rarely appears in a sustainable form close to the ground surface, thus making it difficult for birds to master and use such skill. However, stable wind fields with negative wind shear do exist at higher altitudes. With a growing research on autonomous flight applications at high altitude, possibly all the way to the stratosphere, it is of interest to investigate the possibility of energy extraction from negative wind shear. Results show that it is possible to extract energy from negative shear. It is also revealed that U-shape energy-neutral trajectories are possible for some boundary conditions. These types of trajectories are new and have not been reported in the dynamic soaring literature.

This note begins with an overview of the aircraft mathematical model used to study dynamic soaring as an optimal control problem. This is followed by a description of the numerical optimal trajectory algorithm. Results are presented for a representative glider in practical wind shear conditions.

II. Wind Model

The atmospheric wind velocity is assumed to lie in the horizontal plane along the x direction. The wind speed is considered to vary linearly with altitude with constant gradient β . Accordingly, different cases of the wind profile are considered in this work. First, the case of unrestricted positive shear (wind speed increases with altitude) is considered. Second, the case of altitude-limited positive shear (positive wind shear within a band of altitude of height ΔH) is considered. The associated optimization problems are formulated such that, for each predetermined altitude limit ΔH , the wind shear value is minimized with the optimal trajectory subject to the altitude limit $\max(z) - \min(z) \leq \Delta H$. Third, the case of direction changing wind shear is considered. In such a case, apart from the variation of the wind speed with altitude, it is assumed that the direction of the wind shear also varies linearly with altitude, with a constant gradient p . Finally, the case of negative shear (decreasing wind speed when altitude increases) is considered.

Figure 1 depicts the different cases of wind profile considered in this paper. In general, a wind profile can be written for all the preceding cases by considering that atmospheric wind speed and direction are both linear functions of altitude. To this end, let W be the speed of the wind, and let λ be the angle that the wind velocity vector makes with the x axis in the $x-y$ plane. It is assumed that, according to our convention, W and λ are approximated by affine functions of altitude h as in Eqs. (1) and (2). Note that $h = -z$. Also, it is assumed that the wind speed W is always positive. In other words, it is assumed that

$$W(h) = W_0 + \beta(h - h_0) \geq 0 \quad (1)$$

$$\lambda(h) = p(h - h_0) \quad (2)$$

where β is the wind shear, and p is the wind direction slope. We assume that $\lambda(h_0) = 0$, and $\lambda(h_{\max}) = \lambda_{\max}$. The components of the wind velocity along the x , y , and z inertial directions are then given by

$$W_x = W \cos \lambda, \quad W_y = W \sin \lambda, \quad W_z = 0 \quad (3)$$

Hence, $\dot{W}_z = 0$ and

$$\dot{W}_x = \frac{dW_x}{dh} \frac{dh}{dt} = -V_W \sin \theta_w (\beta \cos \lambda - W p \sin \lambda) \quad (4)$$

and similarly,

$$\dot{W}_y = \frac{dW_y}{dh} \frac{dh}{dt} = -V_W \sin \theta_w (\beta \sin \lambda + W p \cos \lambda) \quad (5)$$

Received 18 May 2017; revision received 22 July 2017; accepted for publication 24 July 2017; published online 31 August 2017. Copyright © 2017 by the American Institute of Aeronautics and Astronautics, Inc. All rights reserved. All requests for copying and permission to reprint should be submitted to CCC at www.copyright.com; employ the ISSN 0731-5090 (print) or 1533-3884 (online) to initiate your request. See also AIAA Rights and Permissions www.aiaa.org/randp.

*R&D Engineer, Corporate Research and Innovation, Halliburton; yiming.zhao@iecc.com.

†Assistant Professor, Department of Aerospace Engineering; atri.dutta@wichita.edu. Senior Member AIAA.

‡Professor, School of Aerospace Engineering; tsiotras@gatech.edu. Fellow AIAA.

§Professor, School of Aerospace Engineering; mark.costello@ae.gatech.edu. Associate Fellow AIAA.

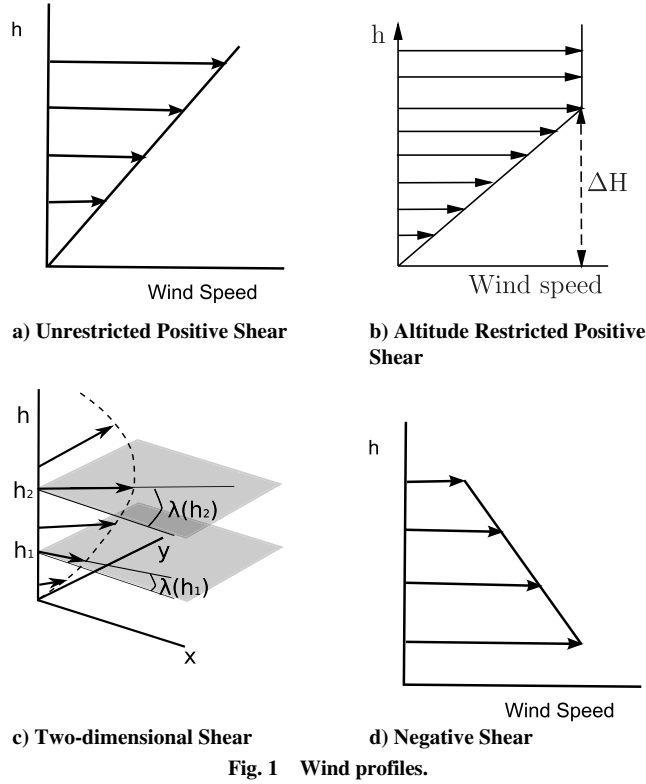


Fig. 1 Wind profiles.

Note that, for the case where the wind does not change direction, we simply have $\lambda = 0$ for all h . Hence, the four cases of wind profile can be written as: 1) unrestricted positive shear: $\beta > 0$, $W_0 = 0$, $\lambda = 0$ for all h , $\Delta H = \infty$; 2) altitude restricted positive shear: $\beta > 0$, $W_0 = 0$, $\lambda = 0$ for all h , ΔH finite; 3) direction changing wind shear: $\beta > 0$, $W_0 = 0$, $\lambda > 0$, $p > 0$; and 4) negative shear: $\beta < 0$, $\lambda = 0$ for all h . Note that, other than β , W_0 also affects whether an energy-neutral loitering pattern exists. Therefore, for a fair comparison with other cases, we also require that the minimum wind speed along the trajectory is zero in case 4.

III. Flight Dynamic Model

As is typical for aircraft trajectory optimization, the motion of the aircraft is modeled by a point mass with inertial position vector components (x, y, z) , where x and y lie in the ground plane, and z is the vertical distance defined as positive down. Forces that drive the motion of the aircraft include gravity, lift, and drag. It is useful to describe the aerodynamic velocity vector in terms of its direction and magnitude. Let the wind speed vector be $W = (W_x, W_y, W_z)$. The air speed V_W is the magnitude of the aerodynamic velocity vector $V_W = (\dot{x} - W_x, \dot{y} - W_y, \dot{z} - W_z)$ and is given by

$$V_W = \sqrt{(\dot{x} - W_x)^2 + (\dot{y} - W_y)^2 + (\dot{z} - W_z)^2} \quad (6)$$

The orientation of the aerodynamic vector V_W can be defined using two Euler angle rotations ψ_W and θ_W , as shown in Fig. 2. The definition of the Euler angles ψ_W and θ_W are given by Eqs. (7) and (8), respectively:

$$\psi_W = \tan^{-1} \left(\frac{\dot{y} - W_y}{\dot{x} - W_x} \right) \quad (7)$$

$$\theta_W = \tan^{-1} \left(\frac{\dot{z} - W_z}{\sqrt{(\dot{x} - W_x)^2 + (\dot{y} - W_y)^2}} \right) \quad (8)$$

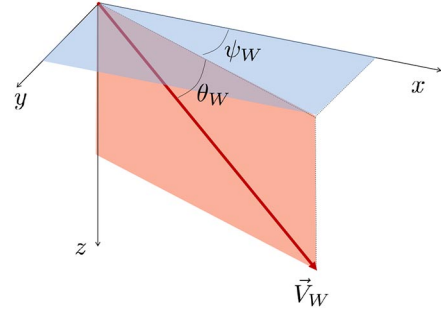


Fig. 2 Wind velocity vector.

The aircraft equations of motion including weight, lift, and drag with atmospheric winds are then given by Eqs. (9–11):

$$m\ddot{x} = \frac{1}{2}\rho V_W^2 S (-\cos\theta_W \cos\psi_W C_D + (\cos\phi \sin\theta_W \cos\psi_W - \sin\phi \sin\psi_W) C_L) \quad (9)$$

$$m\ddot{y} = \frac{1}{2}\rho V_W^2 S (-\cos\theta_W \sin\psi_W C_D + (\cos\phi \sin\theta_W \sin\psi_W + \sin\phi \cos\psi_W) C_L) \quad (10)$$

$$m\ddot{z} = \frac{1}{2}\rho V_W^2 S (-\sin\theta_W C_D - \cos\phi \cos\psi_W C_L) + mg \quad (11)$$

In the preceding equations, the drag coefficient is given by

$$C_D = C_{D0} + K C_L^2 \quad (12)$$

where K and C_{D0} are constants. The aircraft bank angle ϕ and lift coefficient C_L are used as controls.

Rather than use the three second-order equations of motion in Eqs. (9–11), it is more convenient to employ a set of six first-order state equations as given next, which can be derived using Eqs. (9–11) and the definitions of V_W , ψ_W , and θ_W :

$$\dot{x} = V_W \cos\theta_W \cos\psi_W + W_x \quad (13)$$

$$\dot{y} = V_W \cos\theta_W \sin\psi_W + W_y \quad (14)$$

$$\dot{z} = V_W \sin\theta_W + W_z \quad (15)$$

$$\dot{V}_W = -\frac{\rho S V_W^2}{2m} C_D + g \sin\theta_W - \cos\psi_W \cos\theta_W \dot{W}_x - \sin\psi_W \cos\theta_W \dot{W}_y - \sin\theta_W \dot{W}_z \quad (16)$$

$$\dot{\theta}_W = -\frac{\rho S V_W C_L \cos\phi}{2m} + \frac{g}{V_W} \cos\theta_W + \frac{1}{V_W} (\dot{W}_x \sin\theta_W \cos\psi_W + \dot{W}_y \sin\theta_W \sin\psi_W - \dot{W}_z \cos\theta_W) \quad (17)$$

$$\dot{\psi}_W = \frac{\rho S V_W}{2m \cos\theta_W} C_L \sin\phi + \frac{1}{V_W \cos\theta_W} (\sin\psi_W \dot{W}_x - \cos\psi_W \dot{W}_y) \quad (18)$$

IV. Optimal Trajectory Computation

The flight dynamic model [Eqs. (13–18)] is employed to compute optimal aircraft trajectories. In particular, the minimum amount of wind shear required by the aircraft for dynamic soaring is of interest because the knowledge of minimum shear indicates the feasibility of sustaining a dynamic soaring trajectory.

A. Optimization Problem

To compute an optimal aircraft trajectory, appropriate boundary conditions associated with a specific dynamic soaring pattern must be enforced. Among the different dynamic soaring trajectories that are possible, our specific interest lies in the loitering dynamic soaring pattern. For a loitering trajectory, where it is desired that the aircraft remains in a specific geographic region but employs atmospheric wind energy to remain aloft, a periodic trajectory is desired. It is assumed that initially the aircraft is located at the origin of the global coordinate system. It follows that

$$x(0) = 0, \quad y(0) = 0, \quad z(0) = 0 \quad (19)$$

Figure 3 depicts two cases of dynamic soaring loitering patterns. In the first case, the aircraft returns to its original position. Such a case is referred to as energy-neutral case. It corresponds to the case where the energy gained from atmospheric wind is just enough to sustain motion. In the second case, the aircraft is able to gain altitude at the end of the cycle. An altitude gain is possible only when the wind shear is greater than the minimum required one to sustain loitering motion. In this paper, because we are interested in the feasibility of dynamic soaring in a given wind field, only energy-neutral loitering trajectories are considered. The optimal aircraft trajectories are therefore constrained as follows:

$$h(t) = -z(t) \geq 0, \quad \text{for all } t \geq 0 \quad (20)$$

The aerodynamic requirements for the aircraft are formulated as control constraints for the optimization problem required to compute an optimal trajectory:

$$C_L^{\min} \leq C_L \leq C_L^{\max} \quad (21)$$

$$-\phi_{\min} \leq \phi \leq \phi_{\max} \quad (22)$$

The periodic boundary conditions required for a loitering trajectory are

$$V_w(t_f) = V_w(0) \quad (23)$$

$$\psi(t_f) = \psi(0) + 2\pi, \quad \theta_w(t_f) = \theta_w(0) \quad (24)$$

$$x(t_f) = x(0), \quad y(t_f) = y(0), \quad z(t_f) = z(0) \quad (25)$$

To compute an optimal trajectory, a suitable performance index needs to be minimized. In this paper, the minimum shear required to

sustain a loitering dynamic soaring trajectory is of interest because it is indicative of whether energy gain from the wind field is achievable and can act as an explicit metric driving real-time flight control decisions. Therefore, the following objective function is employed:

$$\min_{C_L, \phi} |\beta|, \quad \beta \equiv \text{wind shear} \quad (26)$$

B. Solution Methodology

For the numerical solution of the optimal control problem, a direct optimization scheme is employed. The time interval $[0, t_f]$ is discretized into a grid of points:

$$t_1 < t_2 < \dots < t_f \quad (27)$$

The state and control variables are parameterized with respect to this time grid. This leads to the formation of a parameter optimization problem, which is solved using the optimization software package SNOPT [18]. A multiresolution mesh refinement algorithm is used to improve the grid [19]. At each level of refinement, the parameter optimization problem is solved iteratively until the selected convergence criteria are satisfied. The numerical solution is somewhat sensitive to the initial guess required to compute the optimal trajectory. Different sets of initial guesses are provided together with associated boundary conditions for each dynamic soaring scenario. Also, the standard nondimensionalization technique described in [20] is used along with scaling of the variables to facilitate the convergence of the optimization problem.

V. Results

In this section, example results are shown for a high-performance glider with a mass of 113.0 kg, a wing span of 15.0 m, and a wing area of 5.77 m². The aerodynamic properties of the aircraft are given by $K = 0.02$, $C_{D_0} = 0.0013$. The lift coefficient control is limited to lie in the range of -0.5 to 1.75 , whereas the bank angle control is limited to lie in the range -90 to 90 deg. For all trajectories, the air density is set to standard sea level conditions of 1.29 kg/m^3 . Optimal energy-neutral trajectories are computed for conventional shear, altitude limited shear, direction changing shear, and negative shear.

For the given data previously, the minimum wind shear required to sustain a loitering trajectory is $0.0404/\text{s}$. Figures 4–6 depict this trajectory, which has a cycle time of 26.77 s . The three-dimensional (3-D) optimal loitering trajectory is shown in Fig. 4. The height of the loop is 329 m . The bottom arrow indicates the location and flying direction of the glider at $t = 0$. The glider moves clockwise along the loop when looking from the top. We will refer to this trajectory as the nominal trajectory. It takes the aircraft 15.5 s to climb up the first half

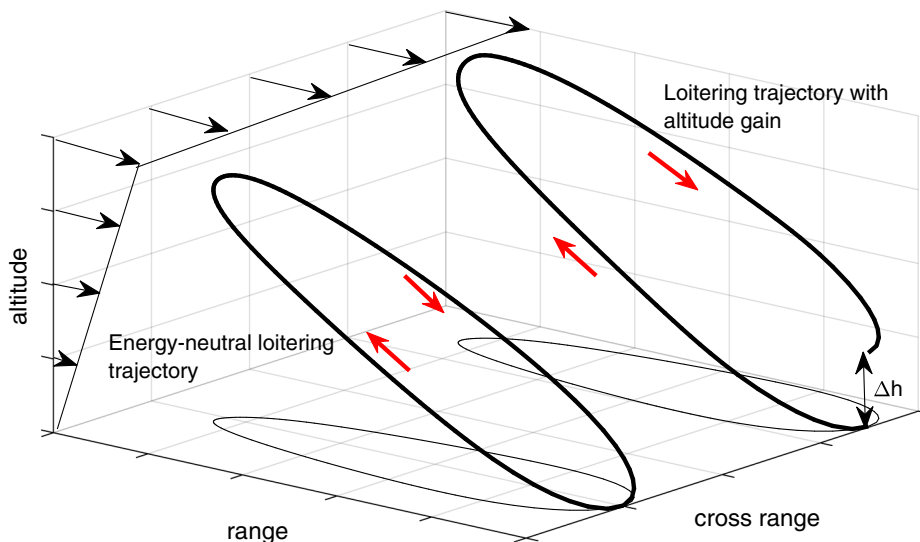


Fig. 3 Loitering patterns of dynamic soaring.

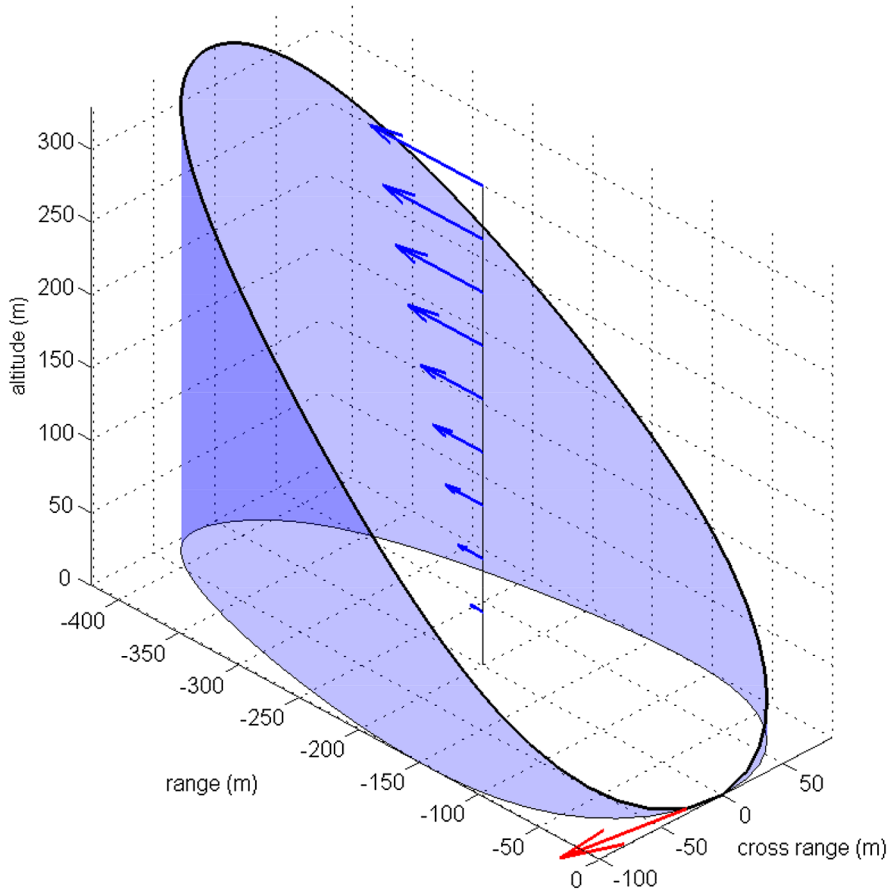


Fig. 4 Energy-neutral optimal loitering trajectory (wind shear = 0.0404 s^{-1}).

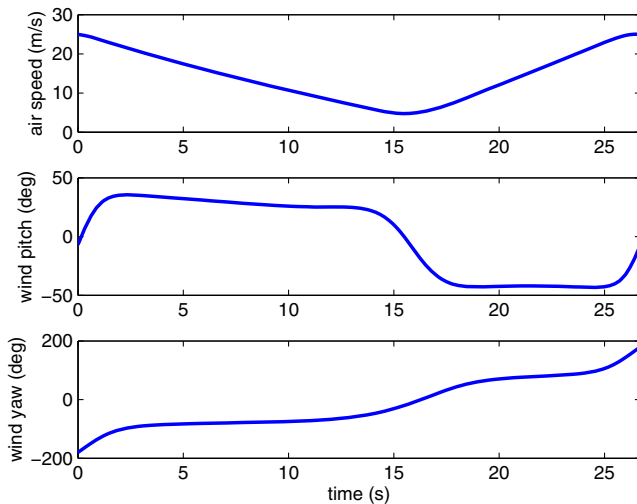


Fig. 5 Energy-neutral optimal loitering trajectory states (wind shear = 0.0404 s^{-1}).

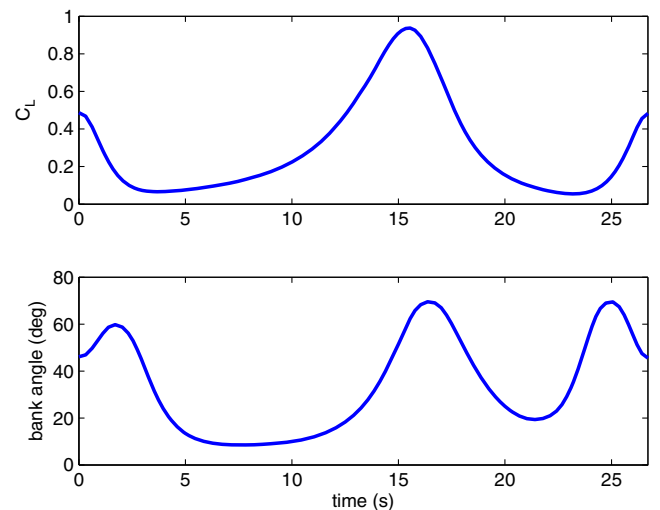


Fig. 6 Energy-neutral optimal loitering controls (wind shear = 0.0404 s^{-1}).

of the loop in tailwind and 11.3 s to finish descent along the rest of the loop in head wind. Because of the symmetry of the problem, there also exists an optimal counterclockwise loop with the same minimum wind shear value, which has been confirmed by numerical optimization using different initial guesses. Figures 5 and 6 depict the variation of the states and controls for the optimal trajectory.

The initial guess used to compute majority of the solutions presented in this paper are as follows [20]:

$$x(t) = \cos(2\pi t/t_f) - 1, \quad y(t) = 0, \quad z(t) = 0 \quad (28)$$

$$\begin{aligned} V_W(t) &= 30.5(2 + \cos 2\pi t), & \theta_W(t) &= 30^\circ \sin 2\pi t/t_f, \\ \psi_W(t) &= -2\pi \sin(\pi t/2t_f) \end{aligned} \quad (29)$$

$$\begin{aligned} x(0) &= x(t_f), & y(0) &= y(t_f), & z(0) &= z(t_f), \\ V_W(0) &= V_W(t_f), & \theta_W(0) &= \theta_W(t_f) \end{aligned} \quad (30)$$

With the preceding initial solutions, one needs to provide only the initial values of V_0 , ϕ , C_L , and t_f [20].

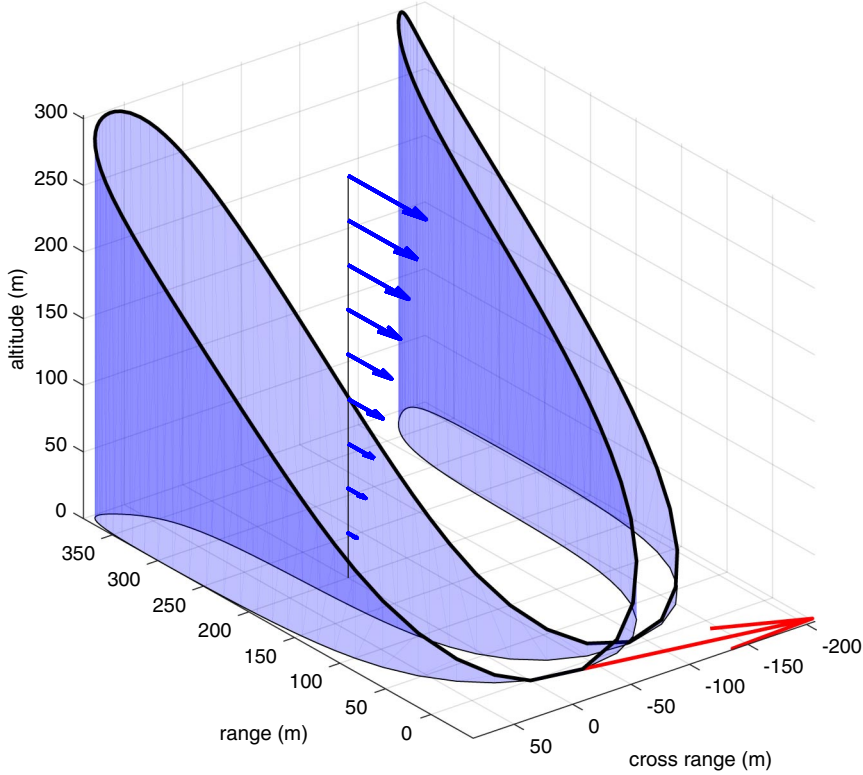


Fig. 7 Energy-neutral optimal U-shape trajectory (wind shear = 0.0397 s⁻¹).

By using a different set of initial guesses and boundary conditions, as in Eqs. (31–33), a U-shaped closed-loop trajectory is obtained, which has not been reported in the literature to the authors’ knowledge. The energy conversion process for the U-shaped trajectory is similar to that of the loiter trajectory, but instead of closing the loop with a 2π heading angle change, the U-shaped trajectory can be broken into two parts (which are almost mirror images of each other), and by traveling along each part, the heading angle of the glider changes by 180 deg, or -180 deg, and the accumulated change of the heading angle is zero during the whole flight. The solution of the minimum shear problem for the U-shaped trajectory is $\beta = 0.0397$, which is smaller than the minimum shear associated with the loitering case. The state and control histories for

this trajectory are shown in Figs. 7–9. The total travel time along the U-shaped trajectory is 50.3 s, and the maximum height of the loop is 311.9 m, which is slightly lower than the loitering case. The periodic motion is sustained in a smaller amount of wind shear by taking advantage of the higher lift available; comparing Figs. 6 and 9, it can be seen that the lift coefficient reaches a higher maximum value than that for the nominal trajectory. It is noted that the state and control along the trajectory are almost symmetric. The initial guess used for obtaining the U-shaped trajectory is as follows:

$$\begin{aligned} x(t) &= -366\sin^2(2\pi t/t_f), & y(t) &= 122\sin(2\pi t/t_f), \\ z(t) &= 244\sin^2(2\pi t/t_f) \end{aligned} \quad (31)$$

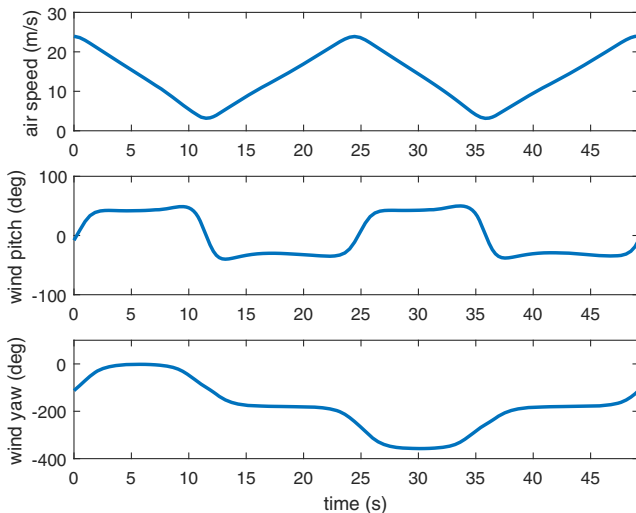


Fig. 8 Energy-neutral optimal U-shape trajectory states (wind shear = 0.0397 s⁻¹).

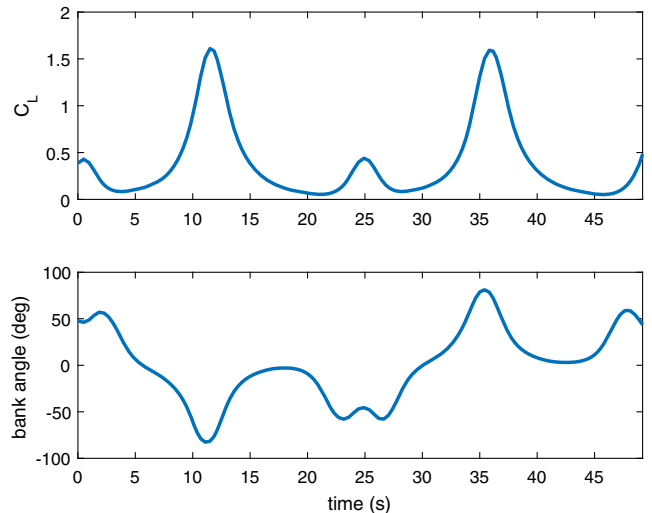


Fig. 9 Energy-neutral optimal U-shape trajectory controls (wind shear = 0.0397 s⁻¹).

$$V_W(t) = 15.3 + 61\cos^2(4\pi t/t_f), \quad \theta_W(t) = 0.2 + 0.5 \sin(4\pi t/t_f),$$

$$\psi_W(t) = -2\pi \sin(\pi t/t_f) \quad (32)$$

and the boundary conditions are

$$\theta_W(0) = \theta_W(t_f), \quad C_L(0) = C_L(t_f), \quad V_W(0) = V_W(t_f),$$

$$\phi(0) = \phi(t_f) \quad (33)$$

Figure 10 shows the scenario where wind shear is only available in a limited altitude band. Optimal trajectories were computed for this case as a function of the altitude band where shear is present, and results are given in Figs. 11 and 12. The effect of decreasing the altitude band where shear is present is to shrink the trajectory so that the (periodic) trajectory occurs within the given shear altitude. Furthermore, Fig. 13 shows that the required wind shear increases exponentially as the wind shear altitude band decreases. It needs to be pointed out that results in Figs. 11 and 12 are obtained by placing hard bounds on state z . Therefore, the minimum shear results shown here are on the conservative side because, in reality, the glider always has the option to fly out of the altitude bound if this benefits the establishment energy-neutral dynamic soaring trajectories.

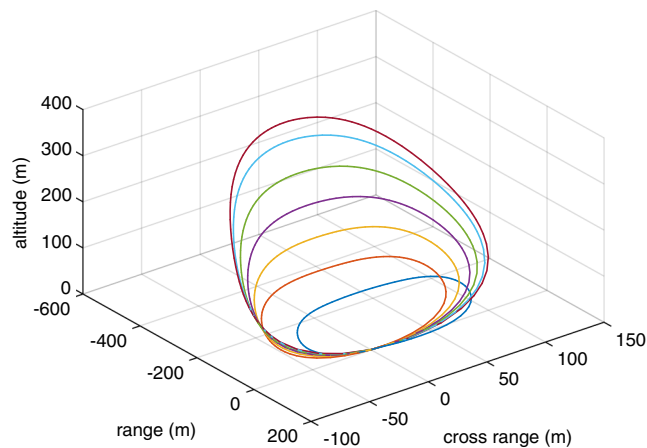


Fig. 10 Energy-neutral optimal trajectories with altitude limited wind shear.

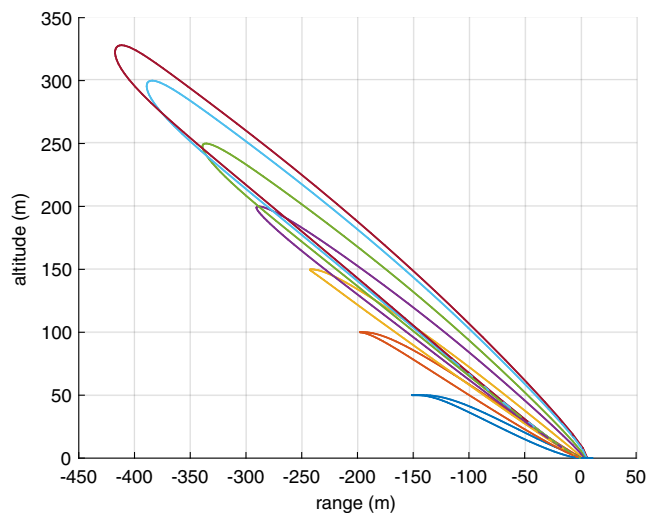


Fig. 11 Energy-neutral optimal trajectories with altitude limited wind shear: side view.

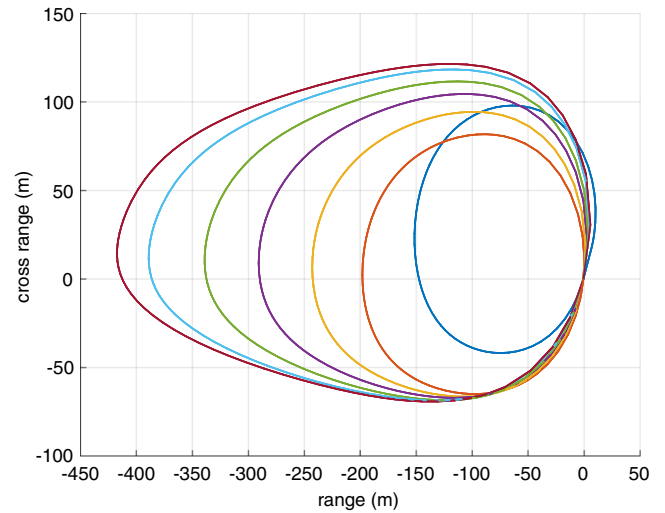


Fig. 12 Energy-neutral optimal trajectories with altitude limited wind shear: top view.

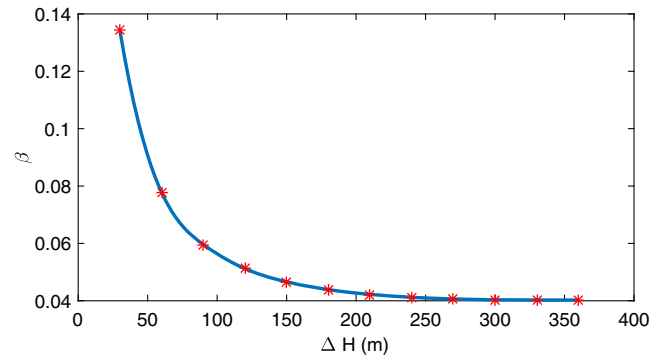


Fig. 13 Altitude limited shear optimal trajectory: minimum shear band.

Figures 14–16 present optimal energy-neutral trajectory results where wind direction changes from 0 to a prespecified maximum angle $\lambda_{\max} = 180$ deg over the altitude of 609.6 m. The same set of initial guess as in dynamic soaring scenario with positive shear is used. When the wind changes direction, the trajectory tilts in the direction of the wind, so as to climb with a head wind, and descends with a tailwind. In this case, the minimum shear value β with varying direction is 0.0313, which is smaller than the minimum shear value with constant wind direction. The lift coefficient, as shown in Fig. 16, reaches the maximum limit for the glider close to the highest point on the trajectory. Thus, changing wind direction can help the glider in extracting energy out of the wind, and a lower level of wind shear is required to sustain the loitering motion of the glider.

In the literature, optimal energy-extraction flight trajectories have considered positive shear where the wind shear speed increases with altitude. It is generally felt that it is not possible to extract energy from negative wind shear structures. The results shown in Figs. 17–19 indicate that it is indeed possible to extract energy from negative shear. Figure 17 shows the negative shear optimal loitering trajectory in 3-D. A similar set of initial guesses as in the positive shear dynamic soaring scenario was used to generate this trajectory, with $\theta_W(t) = -30^\circ \sin 2\pi t/t_f$, and $\psi_W(t) = -2\pi \sin(\pi t/2t_f)$. The total height of the trajectory is 341.9 m, which is slightly higher than the positive shear case. It is enforced in simulation that the wind speed at the highest point of the trajectory is zero. The total cycle time is 27.9 s. The glider spends 15.8 s to climb up the loop in tailwind and return in another 12.1 s heading into the wind. The minimum negative shear found for energy-neutral loiter loops is $\beta = 0.0398 \text{ s}^{-1}$.

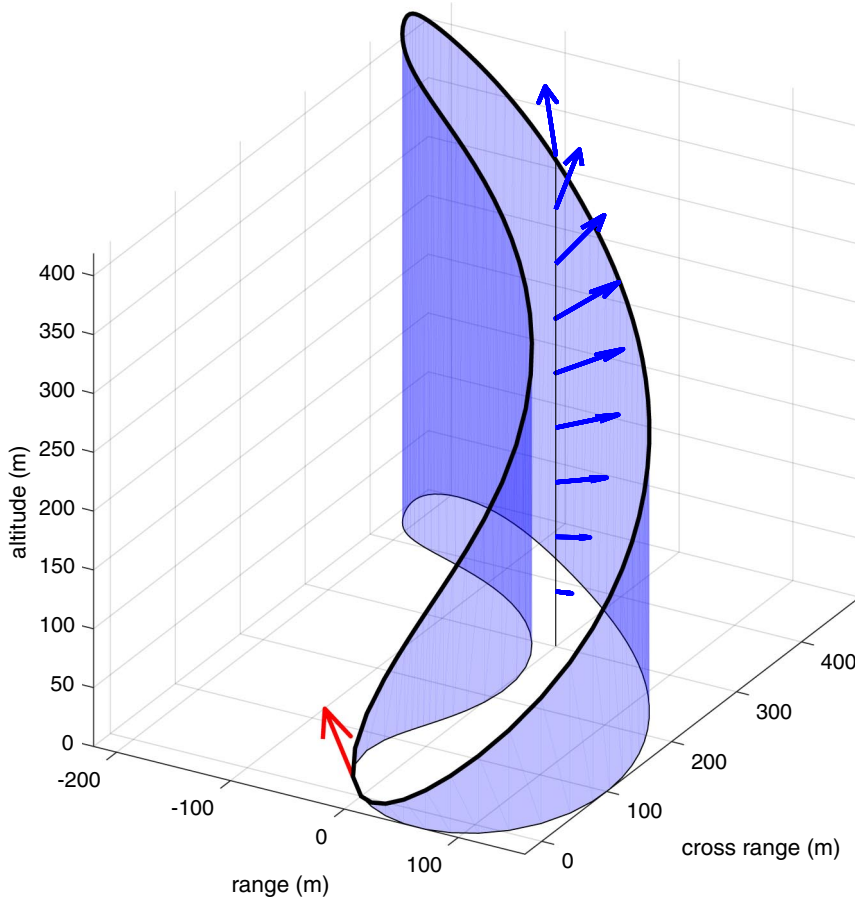


Fig. 14 Energy-neutral optimal loitering trajectory with varying wind direction (wind shear = 0.0313 s^{-1} , $p = 0.2953 \text{ deg/m}$).

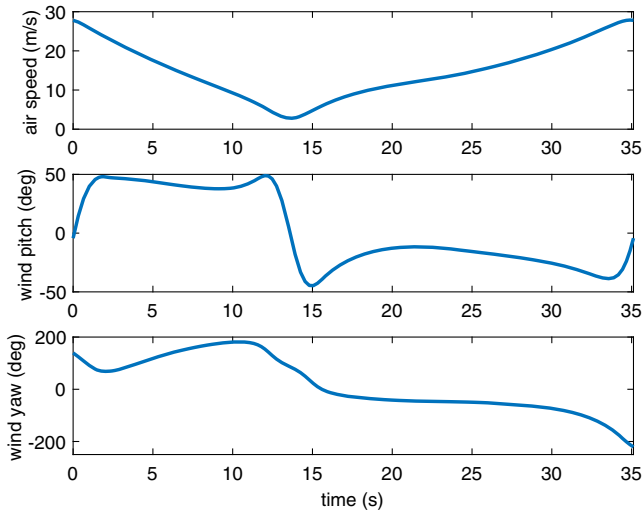


Fig. 15 Energy-neutral optimal loitering trajectory states with varying wind direction (wind shear = 0.0313 s^{-1} , $p = 0.2953 \text{ deg/m}$).

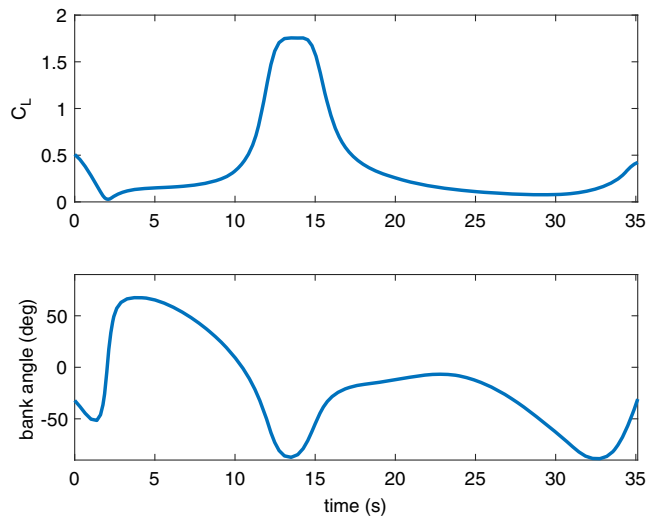


Fig. 16 Energy-neutral optimal loitering controls with varying wind direction (wind shear = 0.0313 s^{-1} , $p = 0.2953 \text{ deg/m}$).

Compared to the positive shear case, and for the same exact conditions (where an energy-neutral trajectory required a wind shear of 0.0404 s^{-1}), it is seen that it is equally possible to extract energy from a wind field with negative shear.

Different tradeoff trends between potential and kinetic energies are observed for different optimal trajectories. As an example, Fig. 20 illustrates the energy tradeoffs for the positive shear case. In this figure, E_k and E_p are the kinetic and potential energies of the glider, respectively, and $E = E_k + E_p$ is the total energy. Note that the slope

of the E curve indicates whether the glider is gaining or losing energy. It is seen from this figure that the glider loses energy at the bottom and very top portions of the trajectory when relatively large lift coefficient is applied, leading to accelerated energy loss attributed to large drag force. Similar observations hold for the trajectory in Fig. 14 with varying wind direction and the U-shape trajectory in Fig. 7. The energy tradeoff trend for the negative shear optimal trajectory is slightly different, as shown in Fig. 21. It is seen from this figure that the glider quickly gains energy in the bottom portion of the trajectory

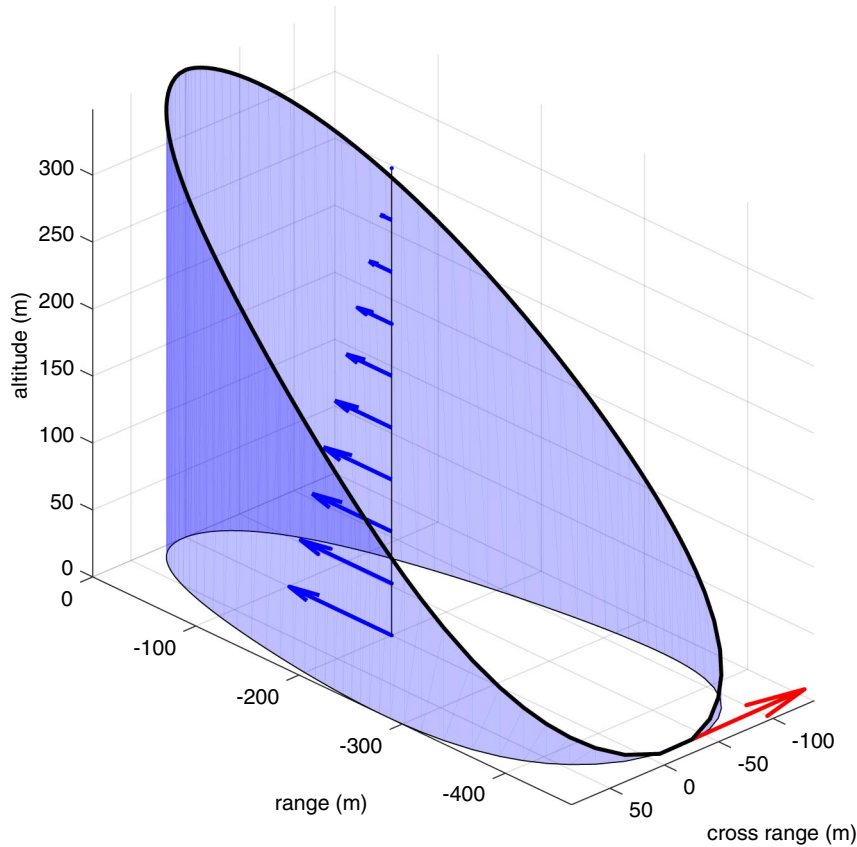


Fig. 17 Energy-neutral optimal loitering trajectory (negative wind shear = 0.0398 s^{-1}).

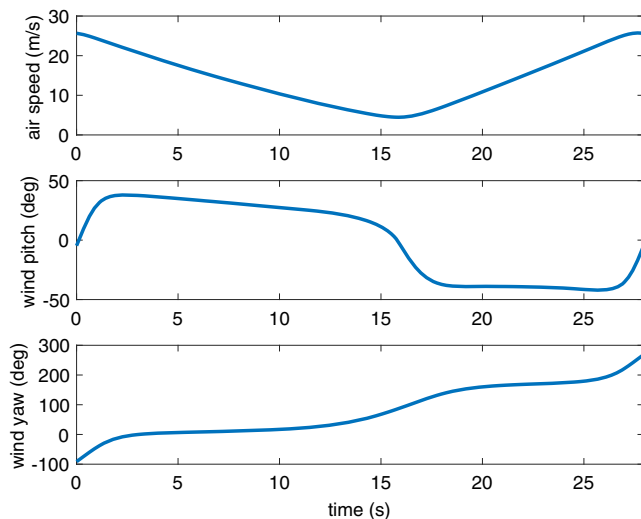


Fig. 18 Energy-neutral optimal loitering trajectory states (negative wind shear = 0.0398 s^{-1}).

when the difference between ground and airspeed is largest due to increased wind speed. In this portion, the aircraft initially increases ground speed by taking advantage of the strong tailwind. After the glider passes the bottom of the trajectory, the glider harvests energy from increased airspeed to gain more altitude. The aircraft is losing energy in other parts of the trajectory when the difference between airspeed and ground speed is small.

Numerical experiments also indicate that aircraft lift-to-drag ratio has considerable impact on the minimum shear value required for energy harvesting from wind field. Table 1 summarizes numerical results of how much the minimum shear value increases relative to the previously documented optimal values (i.e., 0.0402 for the minimum positive shear case, 0.0398

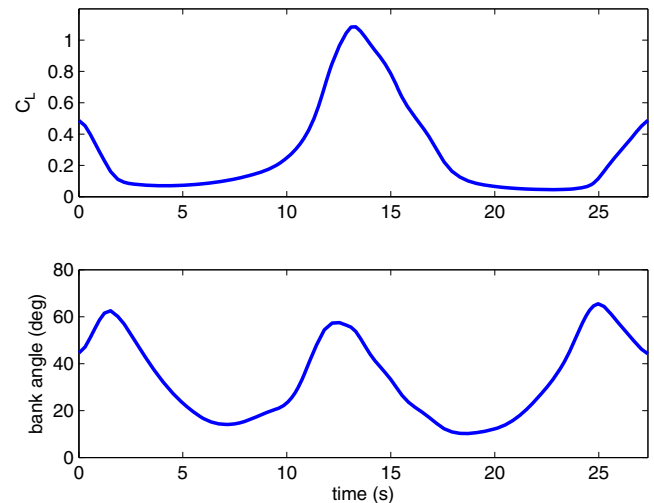


Fig. 19 Energy-neutral optimal loitering controls (negative wind shear = 0.0398 s^{-1}).

for the negative shear case, etc.) when the lift-to-drag ratio is decreased by adjusting both K and C_{D_0} in the same fashion while keeping other aircraft parameters constant. It is seen that the minimum shear is approximately inversely proportional to the lift-to-drag ratio (i.e., a high lift-to-drag ratio is favorable for energy harvesting from wind shear).

VI. Conclusions

Dynamic soaring is a well-known approach of flight, according to which an air vehicle can extract energy from atmospheric wind shear. The typical flight pattern involves maneuvering the aircraft to climb into a head wind shear and dive with a tailwind shear. The bulk of prior research in the literature has considered ideal wind shear where

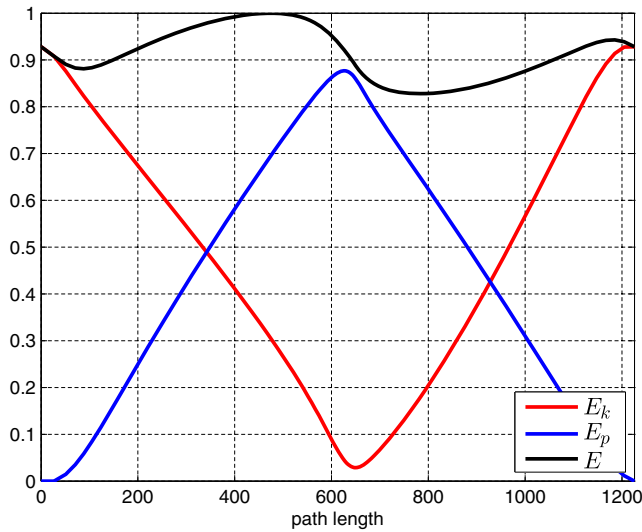


Fig. 20 Energy-neutral optimal loitering energy variation (wind shear = 0.0404 s⁻¹).

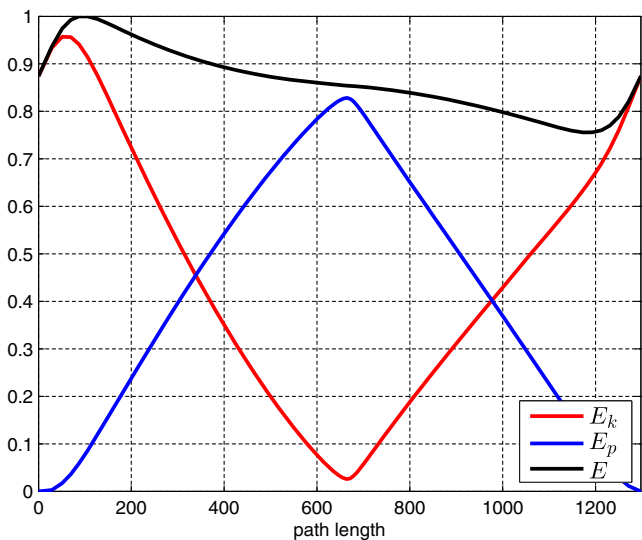


Fig. 21 Energy-neutral optimal loitering energy variation (negative wind shear = 0.0398 s⁻¹).

Table 1 Influence of lift-to-drag ratio on minimum shear for energy-neutral loitering

Lift-to-draft ratio, %	Positive shear, %	Negative shear, %	U-shape, %	Varying direction, %
75	136	134	136	138
50	214	204	212	228

the atmospheric wind shear is available at all altitudes and does not change in direction. Furthermore, all studies to date have considered optimal trajectories where the wind shear is positive, meaning that the atmospheric wind velocity increases with altitude. Generally speaking, when practical atmospheric wind conditions are considered, it is more difficult to achieve dynamic soaring trajectories, and higher levels of wind shear are required to sustain an energy-neutral periodic trajectory. When atmospheric wind shear is present over a limited altitude range and is constant otherwise, the required wind shear increases exponentially as the altitude range decreases. This effect is fairly dramatic and can more than double the required shear levels for maintaining energy-neutral dynamic soaring trajectories. When atmospheric wind direction changes with altitude,

the required shear level for maintaining energy-neutral dynamic soaring trajectories decreases. Our investigation also shows that it is possible to maintain dynamic soaring for both positive as well as negative wind shear, and the required shear level for dynamically soaring in negative shear is slightly lower than the more conventional case of positive wind shear. The optimal trajectories in this note are computed based on parameters for a particular type of glider. For future research, it is desirable to conduct a more comprehensive parametric study to investigate how to expand the operable wind condition from aircraft design perspective, possibly by including aircraft parameters as decision variables in the optimization problem or by comparing optimal trajectories computed using multiple sets of candidate aircraft design parameters.

References

- [1] Metzger, D., and Hedrick, J., "Optimal Flight Paths for Soaring Flight," *Journal of Aircraft*, Vol. 12, No. 11, 1975, pp. 867–871. doi:10.2514/3.59886
- [2] Allen, M., "Guidance and Control of an Autonomous Soaring UAV," NASA TM-2007-214611, Feb 2007.
- [3] Edwards, D., "Implementation Details and Flight Test Results of an Autonomous Soaring Controller," *AIAA Guidance, Navigation and Control Conference and Exhibit*, AIAA Paper 2008-7244, 2008.
- [4] Zhao, Y., "Extracting Energy from Downdraft to Enhance Endurance of Uninhabited Aerial Vehicles," *Journal of Guidance, Control, and Dynamics*, Vol. 32, No. 4, 2009, pp. 1124–1133. doi:10.2514/1.42133
- [5] Andersson, K., and Kaminer, I., "On Stability of a Thermal Centering Controller," *AIAA Guidance, Navigation, and Control Conference*, AIAA Paper 2009-6114, Aug. 2009.
- [6] Rayleigh, L., "The Soaring of Birds," *Nature*, Vol. 27, No. 701, 1883, pp. 534–535. doi:10.1038/027534a0
- [7] Walkden, S., "Experimental Studies of the Soaring Albatrosses," *Nature*, Vol. 116, No. 2908, 1925, pp. 132–134. doi:10.1038/116132b0
- [8] Wilson, J., "Sweeping Flight and Soaring by Albatrosses," *Nature*, Vol. 257, No. 5524, 1975, pp. 307–308. doi:10.1038/257307a0
- [9] Weimerskirch, H., and Robertson, G., "Satellite Tracking of Light-Mantled Sooty Albatrosses," *Polar Biology*, Vol. 14, No. 2, 1994, pp. 123–126. doi:10.1007/BF00234974
- [10] Weimerskirch, H., Bonadonna, F., Bailleul, F., Mabile, G., Dell’Omo, G., and Lipp, H., "GPS Tracking of Foraging Albatrosses," *Science*, Vol. 1259, No. 5558, Feb. 2002, p. 295.
- [11] Hendriks, F., "Dynamic Soaring," Ph.D. Thesis, Univ. of California, Los Angeles, CA, 1972.
- [12] Wurts, J., "Dynamic Soaring," *S&E Modeler Magazine*, Vol. 5, Aug.–Sept. 1998, pp. 2–3.
- [13] Fogel, L., "Dynamic Soaring," *S&E Modeler Magazine*, Vol. 5, Dec.–Jan. 1999, pp. 4–7.
- [14] Boslough, M., "Autonomous Dynamic Soaring Platform for Distributed Mobile Sensor Arrays," Sandia National Lab. TR SAND2002-1896, Albuquerque, NM, 2002.
- [15] Sachs, G., Knoll, A., and Lesch, K., "Optimal Utilization of Wind Energy for Dynamic Soaring," *Technical Soaring*, Vol. 15, No. 2, 1991, pp. 48–55.
- [16] Sachs, G., and Mayrhofer, M., "Dynamic Soaring Basics: Part 1—Model Gliders at Ridges," *Quiet Flyer Magazine*, Kiona Publishing Inc., West-Richland, Dec. 2002, pp. 32–37.
- [17] Sachs, G., and Mayrhofer, M., "Dynamic Soaring Basics: Part 2—Minimum Wind Strength," *Quiet Flyer Magazine*, Kiona Publishing Inc., West-Richland, Jan. 2003, pp. 82–85.
- [18] Gill, P. E., Murray, W., and Saunders, M. A., "SNOPT: An SQP Algorithm for Large-Scale Constrained Optimization," *SIAM Review*, Vol. 47, Jan. 2002, pp. 99–131.
- [19] Jain, S., and Tsiotras, P., "Trajectory Optimization Using Multi-resolution Techniques," *Journal of Guidance, Control and Dynamics*, Vol. 31, No. 5, 2008, pp. 1424–1436. doi:10.2514/1.32220
- [20] Zhao, Y. J., "Optimal Patterns of Glider Dynamic Soaring," *Optimal Control Applications and Methods*, Vol. 25, No. 2, 2004, pp. 67–89. doi:10.1002/(ISSN)1099-1514